Muon spin rotation investigation of the pressure effect on the magnetic penetration depth in $YBa_2Cu_3O_x$

A. Maisuradze,[1,2,*] A. Shengelaya,[3] A. Amato,[1] E. Pomjakushina,[4] and H. Keller[2]

[1]*Laboratory for Muon Spin Spectroscopy, Paul Scherrer Institut, CH-5232 Villigen PSI, Switzerland*
[2]*Physik-Institut der Universität Zürich, Winterthurerstrasse 190, CH-8057 Zürich, Switzerland*
[3]*Department of Physics, Tbilisi State University, Chavchavadze av. 3, GE-0128 Tbilisi, Georgia*
[4]*Laboratory for Developments and Methods, Paul Scherrer Institut, CH-5232 Villigen PSI, Switzerland*

The pressure dependence of the magnetic penetration depth λ in polycrystalline samples of $YBa_2Cu_3O_x$ with different oxygen concentrations $x = 6.45, 6.6, 6.8,$ and 6.98 was studied by muon spin rotation (μSR). The pressure dependence of the superfluid density $\rho_s \propto 1/\lambda^2$ as a function of the superconducting transition temperature T_c is found to deviate from the usual Uemura line. The ratio $(\partial T_c/\partial P)/(\partial \rho_s/\partial P)$ is smaller by a factor of $\simeq 2$ than that of the Uemura relation. In underdoped samples, the zero-temperature superconducting gap Δ_0 and the BCS ratio $\Delta_0/k_B T_c$ both increase with increasing external hydrostatic pressure, implying an increase of the coupling strength with pressure. The relation between the pressure effect and the oxygen isotope effect on λ is also discussed. In order to analyze reliably the μSR spectra of samples with strong magnetic moments in a pressure cell, a special model was developed and applied.

I. INTRODUCTION

The compound $YBa_2Cu_3O_x$ was the first high-temperature superconductor[1] (HTS) with a superconducting transition temperature T_c above the boiling point of liquid nitrogen, and it is one of the most studied HTSs.[2] Its superconducting properties are well characterized, even though some of them are still being heavily discussed. Detailed muon spin rotation (μSR) studies of the magnetic penetration depth λ and the superfluid density $\rho_s \propto 1/\lambda^2$ were performed on polycrystals and single crystals of $YBa_2Cu_3O_x$ at ambient pressure.[3–10] However, the key question concerning the pairing mechanism responsible for high-temperature superconductivity is still not resolved and is the subject of intense debates. Although it is widely believed that magnetic fluctuations play a dominant role in the pairing mechanism,[11] oxygen isotope effect (OIE) studies indicate that lattice degrees of freedom are essential for the occurrence of superconductivity.[12–20] By means of isotope substitution, one can probe the influence of lattice degrees of freedom on superconductivity without changing the lattice parameters.[21] There are no other easily accessible methods which modify only the exchange integral J in order to investigate its influence on the superconducting state.[22] However, the application of hydrostatic pressure changes the interatomic distances in the lattice, which in turn modifies both the lattice dynamics[23] and the exchange coupling J between the Cu spins in cuprates.[24,25] Therefore, a detailed study of the pressure effect (PE) on the superconducting properties (e.g., the superfluid density $\rho_s \propto 1/\lambda^2$, the gap magnitude Δ_0, and the BCS ratio $\Delta_0/k_B T_c$) may provide important information for testing microscopic theories of the high-temperature superconductivity.[26,27]

Up to now, the PE on the superconducting transition temperature T_c was studied by resistivity and Hall effect experiments.[28–31] Several phenomenological[28,32,33] and microscopic models were proposed based on a Hubbard[34,35] or a general BCS approach in order to explain the PE on T_c.[36] The role of nonadiabatic effects is discussed in Ref. 37. These models suggest two basic sources for the PE on T_c: (i) A charge transfer from the charge reservoir to the superconducting CuO_2 plane, which was confirmed by Hall effect experiments,[30,31] and (ii) an increase of T_c due to a pressure-dependent pairing interaction.

The magnetic penetration depth λ is a fundamental parameter of a superconductor. It is a measure of the superfluid density according to the relation $1/\lambda^2 \propto n_s/m^*$, where n_s is the superconducting carrier density and m^* is the corresponding effective mass.[5] From the temperature or field dependence of λ, one can determine the symmetry of the superconducting gap, its magnitude, and the BCS ratio. The pressure dependence of λ was previously studied in fine-powdered grains of $YBa_2Cu_3O_x$[38] and $YBa_2Cu_4O_8$[39–41] by means of magnetization experiments. The μSR technique is a powerful and direct method to determine λ in the bulk of a type II superconductor.[42,43] However, due to several technical difficulties, only a small number of μSR studies of the penetration depth under pressure have been performed so far. The main technical problems are (i) the low fraction of muons stopping in the sample inside the pressure cell and (ii) the strong diamagnetism of a superconductor, which substantially influences the μSR response of the pressure cell.

Here, we report on pressure-dependent magnetic penetration depth studies in polycrystalline samples of $YBa_2Cu_3O_x$ ($x = 6.45, 6.6, 6.8,$ and 6.98) by means of μSR. We found that the pressure-dependent superfluid density $\rho_s \propto 1/\lambda^2$ versus T_c does not follow the Uemura relation.[6] The ratio $\alpha_p = (\partial T_c/\partial P)/(\partial \rho_s/\partial P)$ is smaller by a factor of $\simeq 2$ than that of the Uemura relation but is quite close to that found in oxygen isotope effect (OIE) studies,[16,17] suggesting a strong influence of pressure on the lattice degrees of freedom. Interestingly, a small pressure dependence of the superfluid density was also found in the overdoped sample ($x = 6.98$). The superconducting gap Δ_0 and the BCS ratio $\Delta_0/k_B T_c$ both increase upon increasing the hydrostatic pressure in the underdoped samples, hence implying an increase of the coupling strength with pressure. Finally, a method of data analysis for transverse-field μSR measurements of magnetic

and diamagnetic samples loaded in a pressure cell is presented and applied here. This method leads to a substantial reduction of systematic errors in the data analysis.

The paper is organized as follows: In Sec. II, we give some experimental details. In Sec. III, we describe the method of μSR data analysis and present the experimental results, followed by a discussion in Sec. IV. The conclusions are given in Sec. V. In the appendix, we describe the method used in this work in order to analyze μSR spectra obtained for a magnetic and superconducting sample loaded in a pressure cell.

II. EXPERIMENTAL DETAILS

High-quality polycrystalline $YBa_2Cu_3O_x$ samples with $x = 6.98, 6.8, 6.6$, and 6.45 were prepared from the starting oxides and carbonate Y_2O_3, CuO, and $BaCO_3$ as described elsewhere.[44] Transverse-field (TF) μSR experiments were performed at the μE1 and πM3 beam lines of the Paul Scherrer Institute (Villigen, Switzerland). The samples were cooled in TFs down to 3 K, and μSR spectra were taken with increasing temperature in applied fields $B_{app} = 0.1$ and 0.5 T. Typical statistics for a μSR spectrum were 5–6×10^6 positron events in the forward and backward histograms.[42,43] A CuBe piston-cylinder pressure cell was used with Daphne oil as a pressure-transmitting medium. The maximum pressure achieved was 1.4 GPa at 3 K. The pressure was measured by tracking the superconducting transition of a very small indium plate used as a manometer (calibration constant for In: $\partial T_c / \partial P = -0.364$ K/GPa). In order to avoid charge-transfer effects due to chain reordering in pressurized $YBa_2Cu_3O_x$, the samples were cooled down below 100 K for the μSR measurements within less than 1 h after application of the pressure. This time is much shorter than the time constant $\tau = 27.7$ h (at room temperature) for the pressure-activated chain reordering process.[45] Below 100 K, τ is much longer than the typical measurement time of a sample (<24 h).[45]

High-energy muons ($p_\mu \simeq 100$ MeV/c) were implanted in the sample. Forward and backward positron detectors with respect to the initial muon polarization were used for the measurements of the μSR asymmetry time spectrum $A(t)$ (see Fig. 8 later in this paper).[42] Cylindrically pressed samples were loaded into the cylindrical CuBe pressure cell. The sample dimensions (diameter 5 mm, height 15 mm) were chosen to maximize the filling factor of the pressure cell. The fraction of the muons stopping in the sample was approximately 40%.

III. RESULTS AND ANALYSIS

For type II superconductors in the vortex state in an applied field of $B_{app} \ll B_{c2}$ (B_{c2} is the upper critical field) the square root of the second moment of the muon depolarization rate σ is inversely proportional to the square of the magnetic penetration depth: $\sigma \propto 1/\lambda^2$ (Refs. 4, 46, and 47) and therefore directly related to the superfluid density: $\rho_s \propto 1/\lambda^2 \propto \sigma$. For a polycrystalline sample of a highly anisotropic and uniaxial superconductor, the dominant contribution to the muon depolarization originates from the in-plane magnetic penetration depth $\lambda_{ab} = \lambda_{eff}/1.31$, where λ_{eff} is an effective (averaged) magnetic penetration depth.[48,49]

As was pointed out previously, a substantial fraction of the μSR asymmetry signal originates from muons stopping in the CuBe material surrounding the sample. The sample in the superconducting state induces an inhomogeneous field in its vicinity (see the appendix). This leads to an additional depolarization of the μSR signal arising from the muons stopping in the pressure cell. Therefore, the μSR asymmetry time spectra are characterized by two components and may be described by the following expression:

$$A(t) = A_1 \exp\left(-\frac{1}{2}(\sigma^2 + \sigma_n^2)t^2\right)\cos(\gamma_\mu B_1 t + \phi)$$
$$+ A_2 \exp\left(-\frac{1}{2}\sigma_{pc}^2 t^2\right)\int P(B')\cos(\gamma_\mu B' t + \phi)dB'. \tag{1}$$

Here, A_1 and A_2 are the initial asymmetries of the two components of the μSR signal (A_1, sample; A_2, pressure cell), γ_μ is the gyromagnetic ratio of the muon ($\gamma_\mu = 2\pi \times 135.5342$ MHz/T), and ϕ is the initial phase of the muon spin polarization. B_1 is the field in the center of the sample (or approximately the mean field in the sample). The parameter σ denotes the muon depolarization in the sample due to the field distribution created by the vortex lattice, while $\sigma_n = 0.10(2)$ μs^{-1} is a temperature-, doping-, and pressure-independent depolarization rate due to the nuclear moments present in the sample. The temperature-independent quantity $\sigma_{pc} = 0.27$ μs^{-1} describes the muon-spin depolarization due to the nuclear moments in CuBe. The total asymmetry is $A_1 + A_2 = 0.275$ at 0.1 T and 0.265 at 0.5 T with $A_1/(A_1 + A_2) \simeq 0.4$ ($\simeq$40% of the muon ensemble are stopping inside the sample). $P(B')$ represents the magnetic field distribution probed by the muons stopping in the pressure cell as described in detail in the appendix.

Figure 1 exhibits μSR asymmetry time spectra of $YBa_2Cu_3O_{6.98}$ above ($T = 95$ K) and below ($T = 4.5$ K) the superconducting transition temperature $T_c = 89.6$ K obtained in an applied field of 0.1 T. For better visualization, the spectra and the fits are shown in a rotating reference frame of 0.08 T. Above T_c, only a weak depolarization of the muon spin polarization is visible,[5] while below T_c the strong relaxation of the μSR signal reflects the formation of the vortex lattice in the superconducting state.[3,5,7,43,46] Figures 2(a)–2(c) show the Fourier transforms (FTs) of the μSR time spectra shown in Fig. 1. In Fig. 2(d), the FT spectra of $YBa_2Cu_3O_{6.6}$ below and above $T_c = 60$ K are also shown. The narrow signal around $B_{app} = 0.1$ T in Fig. 2(b) originates from the pressure cell, while the broad signal with a first moment significantly lower than B_{app} arises from the superconducting sample. The signal of the pressure cell is also modified below T_c due to the diamagnetic response of the superconducting sample. The solid lines are the FTs of the fits to the data using Eq. (1) (see also the appendix). The good agreement between the fits and the data demonstrates that the model used here describes the data rather well. The fit of the data for $YBa_2Cu_3O_{6.98}$ measured at $T = 5$ K, $B_{app} = 0.1$ T, and zero pressure with Eq. (1) yields $\sigma = 4.75(15)$ μs^{-1}. In order to test the results obtained with Eq. (1), we performed measurement of the very same $YBa_2Cu_3O_{6.98}$ sample at $B_{app} = 0.1$ T and $T = 5$ K using the low-background spectrometer without pressure cell

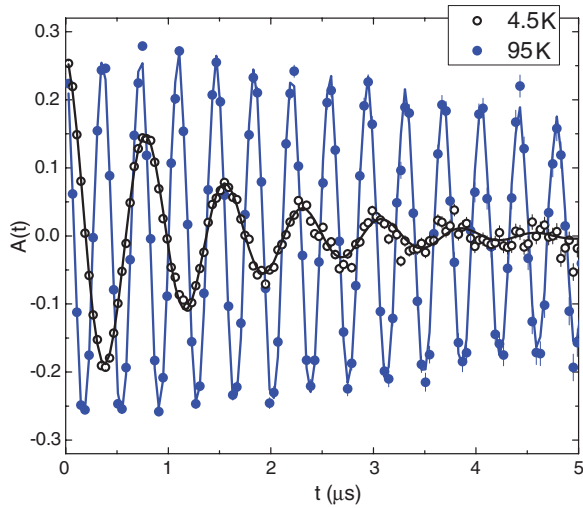FIG. 1. (Color online) μSR asymmetry signal $A(t)$ of YBa$_2$Cu$_3$O$_{6.98}$ measured at $T = 4.5$ K and 95 K in an applied field $B_{\mathrm{app}} = 0.1$ T (empty and full circles, respectively). The fast relaxation of the μSR signal (empty circles) is due to the formation of a vortex lattice in the superconducting state. The solid lines are fits of the data to Eq. (1). For better visualization, the spectra and the fits are shown in a rotating reference frame of 0.08 T.

(GPS, πM3 beamline at PSI, Switzerland). This measurements was analyzed with an equation[50] similar to Eq. (1), resulting in $\sigma = 4.60(7)$ μs^{-1}, which is in good agreement with the result obtained above.

The whole temperature dependence of the μSR asymmetry time spectra was fitted globally with the common parameters B_{app}, A_1, A_2, and σ_n. Solely the parameters B_1 and σ were considered as temperature-dependent free parameters. As shown in the appendix, the field in the sample is macroscopically inhomogeneous due to the inhomogeneity of demagnetization effects. B_1 is the field at the point $x = y = z = 0$ (i.e., the center of the sample). In addition, the parameters describing the muon stopping distribution $x_{0,i}$ and σ_i were kept the same for each temperature scan [see Eqs. (A3) and (A4) in the appendix].

The temperature dependence of the depolarization rates σ for $x = 6.98$, 6.8, 6.6, and 6.45 at $B_{\mathrm{app}} = 0.1$ and 0.5 T obtained with Eq. (1) are shown in Figs. 3 and 4, respectively. The black empty points correspond to the data measured at zero pressure, while the full red points correspond to the data measured at 1.1 GPa (for $x = 6.45$, 6.6, and 6.8) and 1.4 GPa (for $x = 6.98$). The values of T_c and $\sigma(0)$ are in good agreement with previous results.[5,6,8,9] It is known that the order parameter in YBa$_2$Cu$_3$O$_{6.98}$ predominantly has the form of $\Delta = \Delta_0(\hat{p}_x^2 - \hat{p}_y^2)$ ($\hat{p}_i = p_i/|\vec{p}|$ denotes the component of the unit momentum vector in the reciprocal space along the ith axis).[11,51,52] This implies a linear temperature dependence of the superfluid density ρ_s down to very low temperatures due to quasiparticle excitations at the gapless line nodes in the $\hat{p}_x = \pm|\hat{p}_y|$ directions on the Fermi surface.[43] However, in Fig. 3 we clearly see that $\sigma(T)$ tends to saturate at low temperatures for YBa$_2$Cu$_3$O$_{6.98}$ for both applied magnetic fields. Such a behavior was often observed in μSR studies
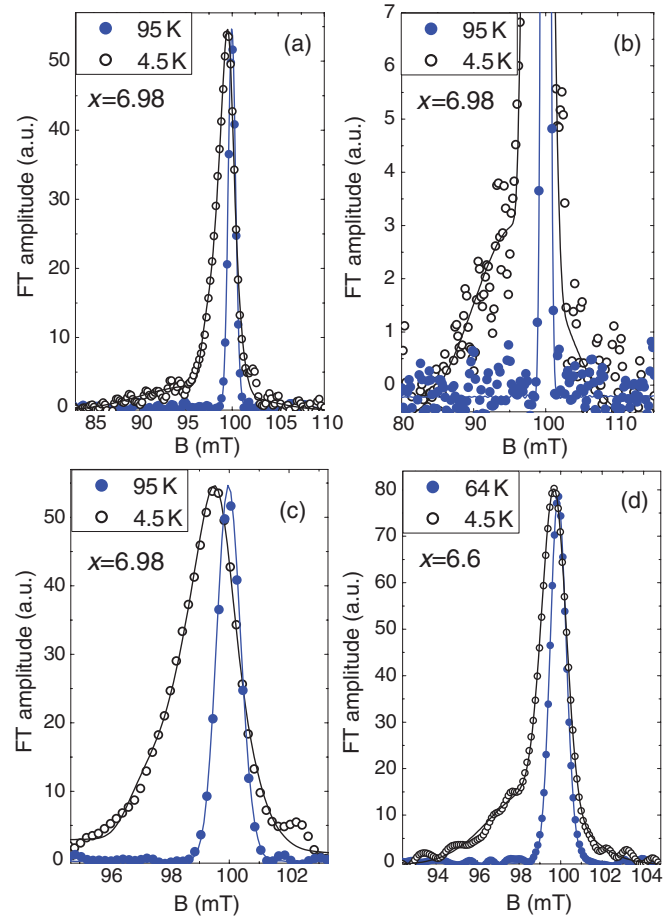

FIG. 2. (Color online) Fourier transform (FT) amplitude as a function of field for the spectra shown in Fig. 1 [panels (a), (b), and (c)]. Panel (b) is the expanded view (along the y axis) of panel (a) showing the signal from the sample. Panel (c) is the expanded view (along the x axis) of panel (a) showing the signal of the pressure cell. Panel (d) shows the FT of the sample with $x = 6.6$ below and above $T_c = 60$ K. The solid lines are the FTs of the fitted curves shown in Fig. 1. The FT spectra are slightly broadened due to a FT apodization of 4 μs^{-1}.

of polycrystalline samples[3,7] and was explained as originating from a strong scattering of electrons on impurities.[53–57]

This scattering can strongly influence the temperature dependence of ρ_s, but it has a minor effect on the superconducting transition temperature T_c. In previous theoretical works, it was suggested that such a behavior indicates scattering in the unitary limit.[55,56] Thus, the temperature dependence of the superfluid density ρ_s was analyzed with the "dirty d-wave model" of the BCS theory in the unitary limit of carrier scattering as described in Ref. 53:

$$\rho_s \propto \frac{1}{\lambda_{ab}^2} = \frac{4\pi e^2 N_f (v_f^{ab})^2}{c^2} \int_0^{2\pi} \frac{d\phi}{2\pi} \sum_{n=0}^{\infty} \frac{|\Delta(\phi)|^2}{(\tilde{\epsilon}_n^2 + |\Delta(\phi)|^2)^{3/2}}. \tag{2}$$

Here, λ_{ab} is the in-plane magnetic penetration depth, $\Delta(\phi) = \Delta_0 \cos(2\phi)g(t)$ ($t = T/T_c$) is the two-dimensional (2D) gap function, and $\tilde{\epsilon}_n = Z(\epsilon_n)\epsilon_n$ are impurity renormalized Matsubara frequencies: $\epsilon_n = (2n + 1)\pi T$. Δ_0 is the maximum
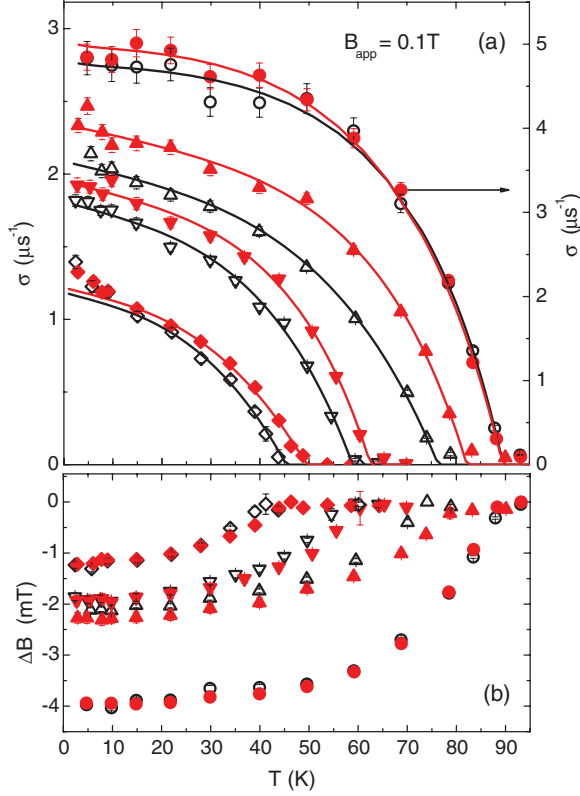
FIG. 3. (Color online) (a) Temperature dependence of σ of YBa$_2$Cu$_3$O$_x$ measured at $B_{\mathrm{app}} = 0.1$ T at zero and applied hydrostatic pressures for $x = 6.45$ ($\diamond$, $P = 0$ GPa; $\blacklozenge$, $P = 1.1$ GPa), $x = 6.6$ ($\triangledown$, $P = 0$ GPa; $\blacktriangledown$, $P = 1.1$ GPa), $x = 6.8$ ($\triangle$, $P = 0$ GPa; $\blacktriangle$, $P = 1.1$ GPa), and $x = 6.98$ ($\circ$, $P = 0$ GPa; $\bullet$, $P = 1.4$ GPa). The data were analyzed with Eq. (1). The solid curves are fits to the data with Eq. (2). (b) Diamagnetic shift of the field $\Delta B = B_1 - B_{\mathrm{app}}$ in the corresponding samples. B_1 is the mean field in the centre of the sample (see text and the appendix).

of the gap function on the Fermi surface, and $g(t)$ represents the temperature dependence of the gap with $g(0) = 1$. The parameters N_f and v_f are the density of states at the Fermi level and the Fermi velocity, respectively. The constants e and c represent the electron charge and the speed of light. The coefficients $Z(\epsilon_n)$ are as follows:[53]

$$Z(\epsilon_n) = 1 + \Gamma_u \frac{D_n(\epsilon_n)Z(\epsilon_n)}{\cot^2(\delta_0) + [D_n(\epsilon_n)\epsilon_n Z(\epsilon_n)]^2}, \quad (3)$$

with

$$D_n(\epsilon_n) = \left\langle \frac{1}{\sqrt{Z(\epsilon_n)^2 \epsilon_n^2 + |\Delta(p_f)|^2}} \right\rangle_{p_f}, \quad (4)$$

and $\delta_0 = \pi/2$ in the unitary limit. The angular brackets $\langle \cdots \rangle_{p_f}$ denote averaging over the Fermi surface. In order to find $Z(\epsilon_n)$ and $g(t)$, Eq. (3) is solved together with the following equation:[53]

$$\frac{1}{2\pi T}\left\{\ln\left(\frac{T}{T_c}\right) + \psi\left(\frac{1}{2} + \frac{\Gamma_u}{2\pi T}\right) - \psi\left(\frac{1}{2} + \frac{\Gamma_u}{2\pi T_c}\right)\right\}$$

$$= \sum_{n=0}^{\infty} \left[\left\langle \frac{|e(p_f)|^2}{\left(Z(\epsilon_n)^2 \epsilon_n^2 + |\Delta(p_f)|^2\right)^{3/2}} \right\rangle_{p_f} - \frac{1}{\epsilon_n + \Gamma_u}\right]. \quad (5)$$
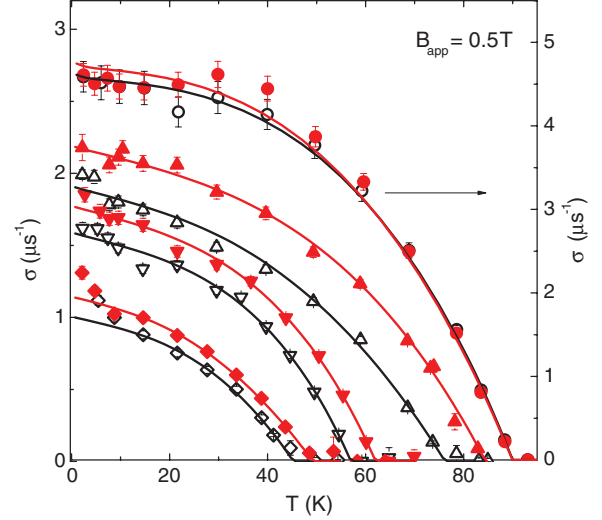

FIG. 4. (Color online) Temperature dependence of σ of YBa$_2$Cu$_3$O$_x$ measured at $B_{\mathrm{app}} = 0.5$ T. The meanings of the symbols and the solid lines are the same as in Fig. 3(a).

Here, $\psi(x)$ is the $\digamma$ function. Note that the impurity scattering influences mainly ϵ_n while the temperature dependence of the gap $g(t)$ changes only slightly for a reasonable scattering rate Γ_u. In the clean limit [i.e., $\Gamma_u = 0$ and $Z(\epsilon_n) = 1$, $\forall n$], the normalized function $g(t)$ is very close to the analytical approximations derived from BCS theory.[58]

Fits of Eq. (2) to $\sigma(T) \propto 1/\lambda_{\mathrm{ab}}(T)^2$ measured at various hydrostatic pressures are presented in Figs. 3 and 4. The corresponding values for Δ_0, T_c, σ_0, and Γ_u obtained from the analysis are summarized in Table I. The data for zero and applied pressure and the same doping x were analyzed simultaneously with the common parameter Γ_u, which characterizes the relaxation rate of the Cooper pairs on impurities. As shown in Table I the data for the underdoped samples ($x = 6.45, 6.6$, and 6.8) are well described by the clean limit d-wave model, while for the overdoped sample ($x = 6.98$) $\Gamma_u = 15(5)$ K. Here, we note that all the studied samples originate from the same batch and have an identical thermal history, except the last process of the oxygen reduction. Therefore, we cannot explain why only the sample with $x = 6.98$ exhibits a saturation of σ in the low-temperature limit and why it has such a high scattering rate $\Gamma_u = 15(5)$ K. Consequently, we cannot exclude the possibility of a modification of the order parameter in overdoped YBa$_2$Cu$_3$O$_x$ where the pseudogap state gradually vanishes. Such a behavior was also observed previously in optimally doped or overdoped polycrystalline samples of YBa$_2$Cu$_3$O$_x$.[3,5,7,8] However, in single-crystal YBa$_2$Cu$_3$O$_x$ close to optimum doping, a linear temperature dependence of $1/\lambda^2$ at low temperatures was also reported.[10,43] For the sample with $x = 6.45$, only the data above 15 K were analyzed, since below 15 K the occurrence of field-induced spin-glass magnetic order hinders a precise determination of σ.

IV. DISCUSSION

The main subject of the present study is the pressure effect on the superconducting gap Δ_0 and the superfluid density

TABLE I. Summary of the results obtained from the temperature dependence of σ at 0.1 and 0.5 T in YBa$_2$Cu$_3$O$_x$ using Eq. (2). Note that for the sample with $x = 6.45$, a precise analysis of σ was not possible due to the occurrence of spin-glass magnetism below $T \simeq 15$ K. Hence, the errors of these values of $\sigma(0)$ are rather large.

x	P (GPa)	B_{app} (T)	T_c (K)	$\sigma(0)$ (μs^{-1})	$\dfrac{\Delta_0}{k_B T_c}$	Γ_u (K)
6.98	0	0.1	89.6(4)	4.76(7)	3.87(12)	15(5)
6.98	1.4	0.1	89.5(4)	4.97(7)	3.60(7)	15(5)
6.98	0	0.5	90.0(2)	4.56(7)	2.95(10)	15(5)
6.98	1.4	0.5	89.9(1)	4.72(7)	2.82(7)	15(5)
6.8	0	0.1	77.1(3)	2.07(5)	3.02(12)	0
6.8	1.1	0.1	83.2(5)	2.33(5)	3.48(15)	0
6.8	0	0.5	76.4(3)	1.91(5)	2.59(9)	0
6.8	1.1	0.5	82.3(5)	2.19(5)	2.80(8)	0
6.6	0	0.1	58.9(6)	1.79(5)	3.02(12)	0
6.6	1.1	0.1	62.6(5)	1.95(5)	3.27(12)	0
6.6	0	0.5	57.3(6)	1.58(5)	2.92(12)	0
6.6	1.1	0.5	62.3(6)	1.77(5)	2.89(11)	0
6.45	0	0.1	45.4(3)	1.17(7)	3.0(5)	0
6.45	1.1	0.1	49.5(5)	1.22(7)	3.0(5)	0
6.45	0	0.5	45.1(2)	1.00(7)	2.5(2)	0
6.45	1.1	0.5	48.7(2)	1.14(7)	2.5(2)	0

FIG. 5. (Color online) T_c vs $\sigma(0)$ (Uemura plot) at zero and applied pressure for YBa$_2$Cu$_3$O$_x$ with $x = 6.45$, 6.6, 6.8, and 6.98. The solid line is the Uemura line while the dashed line is a guide to the eye. The dotted lines represent the pressure effects on T_c and $\sigma(0)$.

$\rho_s \propto \sigma$. The Uemura relation,[6] implying the linear relation between T_c and ρ_s for underdoped cuprate superconductors, was established soon after the discovery of HTS[1] and is one of the important criteria which a microscopic theory of HTS should explain. The Uemura relation for the data summarized in Table I is shown in Fig. 5. As indicated by the dotted lines, the slope $\alpha_p = (\partial T_c/\partial P)/(\partial \sigma/\partial P)$ is systematically smaller than that suggested by the Uemura line with $\alpha_U = \partial T_c/\partial \sigma \simeq 40$ K/μs^{-1}. The values of α_p for the underdoped samples investigated in this work are summarized in Table II. Note that due to magnetism below $\sim$15 K the error of $\sigma(0)$ for the sample with $x = 6.45$ is rather large. The weighted mean value of $\alpha_p \simeq 23(4)$ K/μs^{-1} is a factor of $\simeq$2 smaller than $\alpha_U \simeq 40$ (K μs^{-1}). Such a substantial deviation from the Uemura line (with a lower value of α_p) was also observed by pressure experiments in YBa$_2$Cu$_4$O$_8$ using a magnetization technique.[39] This is in contrast to pressure effect results obtained for the organic superconductor κ-(bis(ethylenedithio)tetrathiafulvalene)$_2$Cu(NCS)$_2$, which follow the Uemura relation.[59] Interestingly, a slope smaller by a factor of 2 than that of the Uemura line was also found by OIE studies of cuprate superconductors.[16] This suggests a strong influence of pressure on the lattice dynamics.

It is known that the pressure dependence of the superconducting transition temperature is determined by two mechanisms: (i) the pressure-induced charge transfer to CuO$_2$ planes Δn_h and (ii) the pairing interaction V_{eff}, which depends on pressure.[28,32–37,60] For the underdoped samples, the former mechanism dominates (85–90%) the pressure effect on T_c.[28,32,36] Therefore, one can separate the pressure effect on σ also in two components: $\Delta\sigma = \Delta\sigma_{ch} + \Delta\sigma_V$. The first term $\Delta\sigma_{ch} \simeq (1/\alpha_U)(\partial T_c/\partial P)P$ follows the Uemura lin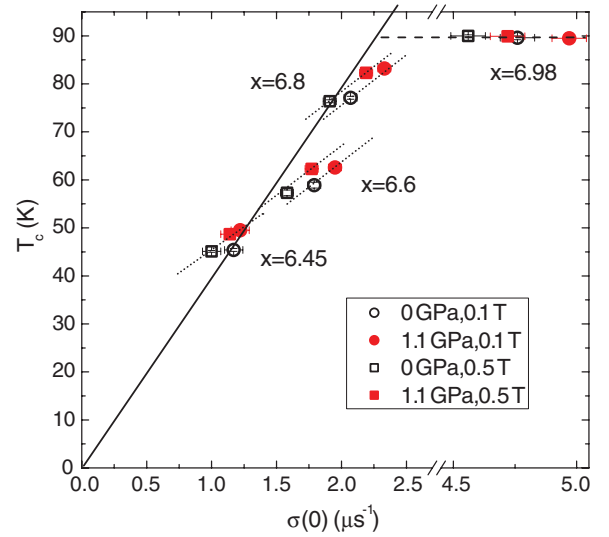e and is mainly due to the charge transfer to the plane. The second term $\Delta\sigma_V \simeq (1/\alpha_p - 1/\alpha_U)(\partial T_c/\partial P)P$ describes the increase of the superfluid density solely due to a change of the pairing interaction. This increase of the superfluid density is equivalent to a decrease of the effective mass of the superconducting carriers, since $\Delta\sigma_V/\sigma = \Delta\lambda_V^{-2}/\lambda^{-2} = -\Delta m_V^*/m^*$.[39] Therefore, the pressure-induced change of the effective carrier mass can be written as

$$d\ln(m_V^*)/dP = -d\ln(\lambda_V^{-2})/dP \equiv -(\Delta\sigma_V/\sigma)/\Delta P$$
$$\simeq (\alpha_U/\alpha_p - 1)(\partial T_c/\partial P)/T_c$$
$$\simeq 3/T_c \text{ GPa}^{-1}. \qquad (6)$$

Here, T_c and σ are taken at zero pressure, and the value of $(\partial T_c/\partial P) \simeq 4$ K/GPa was used. This value is practically doping independent in underdoped YBa$_2$Cu$_3$O$_x$ for $6.45 \leqslant x \leqslant 6.8$.[32] The quantity $\Delta\lambda_V^{-2}$ describes the change of the superfluid density solely due to a modification of the pairing interaction V_{eff} by pressure. It is remarkable to observe the qualitative agreement between $d\ln(\lambda_V^{-2})/dP$ and that found in OIE studies for $d\ln\lambda/d\ln M_O$ at different carrier dopings ($d\ln M_O$ is the relative change of oxygen mass).[16] Indeed, Eq. (6) predicts that the pressure effect on m_V^* strongly increases with decreasing T_c.

TABLE II. Values of $\alpha_p = (\partial T_c/\partial P)/(\partial \sigma/\partial P)$ for the underdoped YBa$_2$Cu$_3$O$_x$ samples investigated in this work ($x = 6.45$, 6.6, and 6.8).

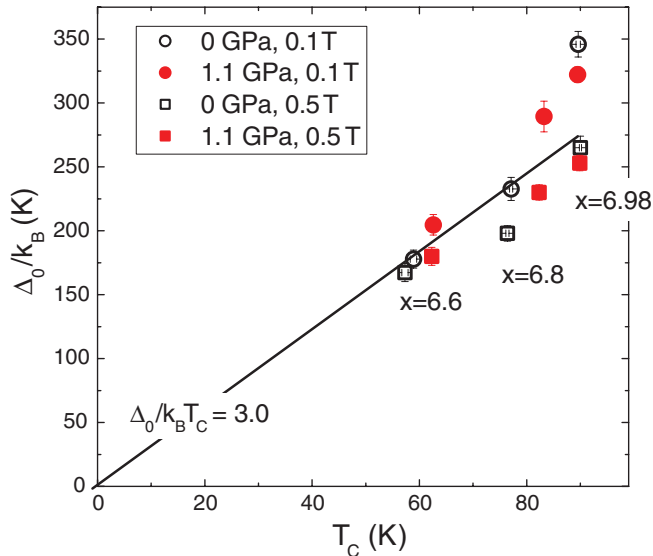| x	α_p (K/μs^{-1}) 0.1 T	α_p (K/μs^{-1}) 0.5 T
6.45	—	25(18)
6.6	23(11)	26(6)
6.8	23(7)	21(6)

FIG. 6. (Color online) Relation between Δ_0 and T_c for YBa$_2$Cu$_3$O$_x$ with $x = 6.6$, 6.8, and 6.98. The solid line corresponds to $\Delta_0/k_B T_c = 3$ (weak-coupling BSC superconductor: $\Delta_0/k_B T_c = 1.76$). Both Δ_0 and $\Delta_0/k_B T_c$ increase with increasing pressure.

FIG. 7. (Color online) The gap Δ_0 as a function of $\sigma(0)$ for the underdoped samples of YBa$_2$Cu$_3$O$_x$ with $x = 6.6$ and 6.8. The linear relation between $\sigma(0)$ and Δ_0 is better fulfilled under hydrostatic pressure than the Uemura relation T_c vs $\sigma(0)$ and $\Delta_0/k_B T_c$ vs T_c (see Figs. 5 and 6). The line is a guide to the eye.

Another interesting result is the quite small pressure dependence of σ in the overdoped sample with $x = 6.98$, which is approximately a factor of $\simeq 2$ weaker than that reported from magnetization measurements.[38] In Fig. 6, the gap magnitudes Δ_0 for the samples with $x = 6.6$, 6.8, and 6.98 are plotted as a function of T_c. For the underdoped samples ($x = 6.6$ and 6.8), both Δ_0 and $\Delta_0/k_B T_c$ increase upon increasing applied pressure. This suggests an increase of the coupling strength with increasing pressure. This behavior is different from that found for the OIE on Δ_0, where a proportionality between Δ_0 and T_c was found, implying a constant ratio of $\Delta_0/k_B T_c$.[18] In the overdoped sample ($x = 6.98$), Eq. (2) suggests a small reduction of the coupling strength with increasing pressure. However, as was mentioned above, the absence of a linear temperature dependence of σ at low temperatures for the sample with $x = 6.98$ might also indicate that the superconducting order parameter is not of purely d-wave character.[51,52] This, on the other hand, may influence the result for Δ_0 and its pressure dependence.

In Fig. 7, for the underdoped samples ($x = 6.6$ and 6.8) Δ_0 is plotted versus $\sigma(0)$, showing a linear correlation between the two quantities. Note that this correlation does not change with the application of hydrostatic pressure. This is in contrast to what is observed for the Uemura relation, T_c versus $\sigma(0)$ and $\Delta_0/k_B T_c$ versus T_c (see Figs. 5 and 6).

V. CONCLUSIONS

The pressure dependence of the magnetic penetration depth λ of polycrystalline YBa$_2$Cu$_3$O$_x$ ($x = 6.45$, 6.6, 6.8, and 6.98) was studied by μSR. The pressure dependence of the superfluid density $\rho_s \propto \sigma \propto 1/\lambda^2$ as a function of the superconducting transition T_c temperature does not
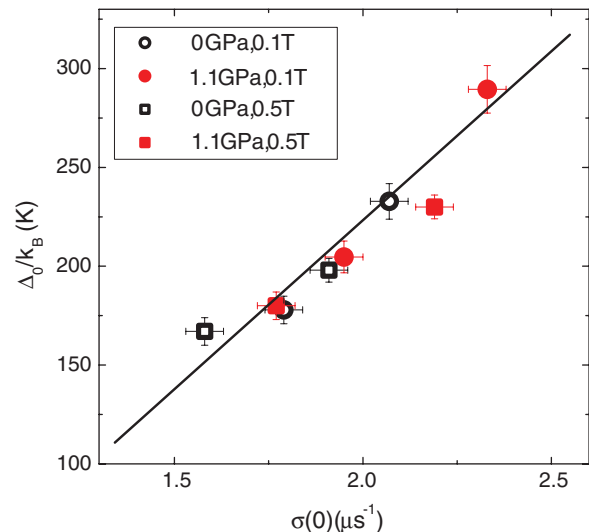
follow the well-known Uemura relation.[6] The ratio $\alpha_p = (\partial T_c/\partial P)/(\partial \sigma/\partial P) \simeq 23(4)$ K/μs^{-1} is smaller by a factor of $\simeq 2$ than that of the Uemura relation observed for underdoped samples. However, the value of α_p is quite close to that found in OIE studies,[16] indicating a strong influence of pressure on the lattice degrees of freedom. We conclude that the contribution of carrier doping to the pressure dependence of λ is similar to the OIE on λ. A weak pressure dependence of the superfluid density ρ_s was found in the overdoped sample ($x = 6.98$). The superconducting gap Δ_0 and the BCS ratio $\Delta_0/k_B T_c$ both increase with increasing applied hydrostatic pressure in the underdoped samples, implying an increase of the coupling strength with pressure. Although the Uemura relation does not hold and the BCS ratio is increasing with pressure in underdoped samples, the relation between Δ_0 and the μSR relaxation rate σ is invariant under pressure. Finally, a model to analyze TF μSR spectra of magnetic and diamagnetic samples loaded into a pressure cell was developed and successfully used in this paper (see the appendix), resulting in a substantial reduction of the systematic errors in the data analysis.

APPENDIX: FIELD DISTRIBUTION IN A PRESSURE CELL LOADED WITH A SAMPLE WITH NONZERO MAGNETIZATION

Samples with a strong magnetization placed in a pressure cell with an applied magnetic field induce a magnetic field in the space around the sample. Typical examples of such samples are superconductors (strong diamagnets), superparamagnets, and ferro- or ferrimagnets. Thus, muons stopping in a pressure cell (PC) containing the sample will undergo precession in the vector sum of the applied field and the field induced by the sample. This spatially inhomogeneous field leads to an additional depolarization of the muon spin polarization, which depends on the applied field and the induced field together with the spatial stopping distribution of the muons.

Consider the simplest case of a sample with the shape of a round cylinder of height H and radius R placed into a cylindrical pressure cell with the same internal radius R [Fig. 8(a)]. Typical pressure cell radii used for μSR studies are $R = 2.5$–4 mm. In standard TF μSR experiments, the pressure cell is placed with the cylinder axis oriented vertically while the magnetic field is applied perpendicular to the cylinder axis of the pressure cell and the muon beam direction (see Fig. 8). Let us introduce a Cartesian coordinate system with the y axis along the sample cylinder axis and the z axis along the direction of the applied field. Thus, the x axis is along the initial muon beam direction, which is perpendicular to

FIG. 8. (Color online) (a) Schematic sketch of the μSR pressure instrument GPD at the Paul Scherrer Institute: Cylindrical sample (S), pressure cell (PC), muon stopping distribution (dotted ellipse), and forward and backward positron detectors. (b) Illustration of the surface current on a slice of a homogeneously magnetized cylindrical sample. The magnetic field induced by this slice is equivalent to the magnetic field of the surface currents. (c) Cross section of the cylindrical sample and the surface current distribution in xz plane. (d) Magnetic field map of the surface currents as illustrated in panels (b) and (c).

the forward and backward detector planes (see Fig. 8). The origin of the coordinate system is located in the center of the sample.

In an applied magnetic field **H** (along the z direction), the sample has a magnetization **M**. This magnetization is the source of an induced field $\mathbf{H}'(\mathbf{r})$. Let us assume that $\mathbf{H}'$ is much weaker that the applied field **H**, which is the case for superconductors in a magnetic field of $\mu_0 H \gg B_{c1}$ (B_{c1} is the first critical field). Thus, one can neglect the spatial variation of the magnetization due to the additional induced field: $M = M[H + H'(\mathbf{r})] \simeq M(H)$. Typically half (or even more) of all the muons are stopping in the PC outside of the sample volume. The muons stopping in the macroscopically inhomogeneous field of the PC contribute to an additional relaxation of the μSR signal. In order to describe the total μSR time spectrum (sample and PC), one has to model the field distribution $\mathbf{H}'(\mathbf{r})$. For an applied field $H \gg H'(\mathbf{r})$, one can neglect the influence of $H'_x(\mathbf{r})$ and $H'_y(\mathbf{r})$ on the μSR time spectrum, since only the z component $H'_z(\mathbf{r})$ contributes significantly to the muon depolarization. The induced magnetic field $\mathbf{H}'(\mathbf{r})$ created by a cylindrical sample can be calculated as follows:[61]

$$\mathbf{H}'(\mathbf{r}) = \frac{1}{4\pi} \int_V \left[\frac{3(\mathbf{M} \cdot (\mathbf{r} - \mathbf{r}'))(\mathbf{r} - \mathbf{r}')}{|\mathbf{r} - \mathbf{r}'|^5} - \frac{\mathbf{M}}{|\mathbf{r} - \mathbf{r}'|^3} \right] d\mathbf{r}'.$$

(A1)

Here, the integral is taken over the sample volume V. For a sample with a constant magnetization, the three-dimensional integral can be replaced by surface integrals. Let us take one slice of width dz out of the sample cylinder and divide it into many small squares $dA = dxdy$ [see Fig. 8(b)]. The field created by the elementary cell of volume $dV = dxdydz$ with magnetization M is equivalent to the field created by the current $I_z = Mdz$ circulating within this square slice, as shown in Fig. 8(a). It is obvious that integration of this field over the whole slice volume will leave only a current I_z flowing over the perimeter of the slice. The total field of the cylinder is the integral of the fields created by these slices with constant current I_z [see Figs. 8(b) and 8(c)].

According to the law of Bio-Savart, the field in a point **r** created by the elementary currents $Id\ell$ at the surface of the cylinder (with coordinates $\mathbf{r_s}$) is[61]

$$\mathbf{H}'(\mathbf{r}) = \oint_S \frac{I}{4\pi} \frac{[d\boldsymbol{\ell_s} \times (\mathbf{r} - \mathbf{r_s})]}{|\mathbf{r} - \mathbf{r_s}|^3}.$$

(A2)

The integration is taken over the surface S of the sample, and $d\boldsymbol{\ell_s}$ is the elementary length on the surface with its direction along the current (the subscript s denotes quantities related to the surfaces of the sample).

The spacial magnetic field distribution around the ferro/paramagnetic sample calculated with Eq. (A2) in xz plane is shown in Fig. 8(d). The total field in the pressure cell is the vector sum of this field and the homogeneous external field. It is obvious from the figure that the field along the z axis is higher (lower) than the external field in a ferromagnet (diamagnet). Along the x axis, on the other hand, the field is lower (higher) than the external field in a ferromagnet (diamagnet). The maximal (minimal) induced field in the PC are just on the border of the sample pressure
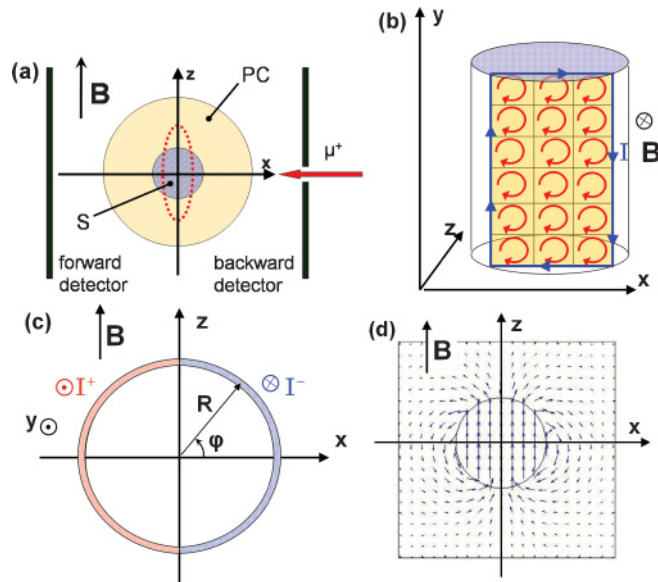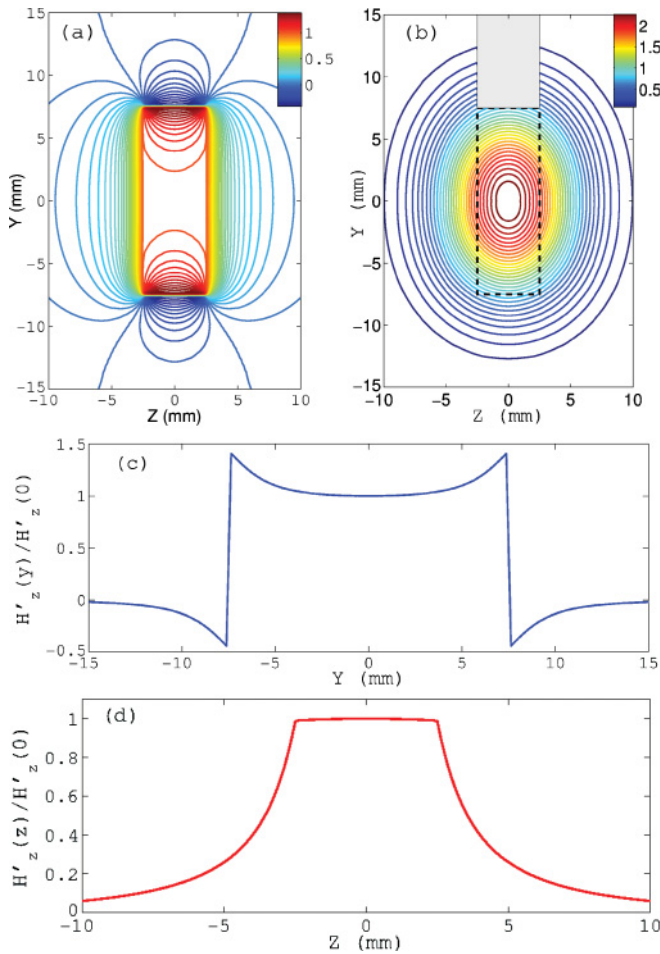
FIG. 9. (Color online) (a) Contour plot of the field distribution $H_z'(y,z)$ in the yz plane for a cylindrical sample with $R = 2.5$ mm and $H = 15$ mm (the geometry of the sample used in the experiment). (b) Contour plot of the muon stopping distribution in the yz plane. The gray area on the top of the sample corresponds to the empty pressure cell space where no muons stop (this space is filled with a low-density pressure transmission medium). The dashed line indicates the sample space. (c) Magnetic field profile of H_z' along the y axis and (d) magnetic field profile of H_z' along the z axis.

cell along z (x) direction. Note that demagnetization effects are naturally accounted for using Eq. (A2). Since the sample is not elliptical, this leads to field inhomogenieties within the volume of the sample (see Fig. 9). As an example, Fig. 9 shows the magnetic field distribution in the yz plane for a cylindrical sample with $H = 15$ mm and radius $R = 2.5$ mm, together with fields along the z and y axes calculated with Eq. (A2). Due to demagnetization effects, the magnetic field profiles within the sample has peaks at the top and bottom edges of the sample where the demagnetizing fields are minimal [Fig. 9(c)]. On the other hand, the field profile within the sample close to the center is quite homogeneous, since a cylinder with infinite height H is equivalent to an ellipsoid in which the field is homogeneous.

In order to calculate the probability field distribution of a sample in a PC with a substantial first moment, a model for the

muon stopping distribution is required. This distribution may be well approximated by a three-dimensional Gaussian:[62]

$$P_s(x_1,x_2,x_3) = \frac{A}{(2\pi)^{3/2}} \prod_{i=1}^{3} \frac{1}{\sigma_i} \exp\left(-\frac{(x_i - x_{0,i})^2}{2\sigma_i^2}\right), \quad \text{(A3)}$$

where the subscripts $i = 1,2,3$ correspond to x, y, and z, respectively. The quantities $x_{0,i}$ determine the mean value of the muon stopping distribution, σ_i are corresponding standard deviations, and A is the normalization factor. The quantities $x_{0,1}$, $x_{0,2}$, and $x_{0,3}$ can be determined quite accurately before starting the experiment by tuning the momentum of the muon beam and vertical positioning of the sample. For a sample with nearly the same density as the pressure cell, $x_{0,1} \simeq x_{0,2} \simeq x_{0,3} \simeq 0$. Simulations of the stopping distribution with the SRIM software[62] yield $\sigma_1 = 0.875$ mm for copper (the basic component of the CuBe pressure cell) and the minimal ratio of $\sigma_3/\sigma_1 = 3.36$. A maximal ratio of $\sigma_3/\sigma_1 \simeq 4$ is estimated for the muon beam collimated by a 4×10 mm collimator (this uncertainty is related to the degree of muon beam focusing). The parameter σ_2 is in fact the standard deviation of the function representing the convolution of a Gaussian with $\sigma = \sigma_3$ over the collimator profile function along the y axis. These parameters define the fraction of muons stopping in the PC and the sample for a given sample geometry. For a known $P_s(\mathbf{r})$, one can calculate the magnetic field probability distribution $P(B)$ in the pressure cell by solving the integral:

$$P(B) = \int_{x^2+z^2>R^2} P_s(\mathbf{r})\delta(B - \mu_0[H + H_z'(\mathbf{r})])d\mathbf{r}. \quad \text{(A4)}$$

Here, $\delta(x)$ is the δ function. The integration is taken over the volume of the pressure cell. Note that this is not simply the probability field distribution in the pressure cell, but it is weighted with the muon stopping probability distribution $P_s(x,y,z)$. Fits of $P(B)$ to the experimental μSR data are shown in Fig. 2. The corresponding temperature-dependent parameters for $B_{app} = 0.1$ T are shown in Fig. 3. The analysis leads to the following temperature-independent parameters for the muon stopping distribution: $x_{0,1} = 0$ mm, $x_{0,2} = 1.7$ mm, $x_{0,3} = 0.03$ mm, $\sigma_1 = 0.875$ mm (this parameter was fixed), $\sigma_2 = 3.1$ mm, and $\sigma_3 = 3.0$ mm. These results are in good agreement with the simulated[62] and partially measured spatial muon stopping distributions. The function $P(B)$ describes the experimentally measured μSR signal rather well.

Below we summarize the influence of a magnetized sample in a pressure cell on the μSR spectrum. As is obvious from Fig. 2, the main influence of the sample is the broadening of the field distribution in the pressure cell with a characteristic shape $P(B)$. This broadening is directly proportional to the magnetization of the sample $\mu_0 M$ or to $B_{app} - B_1 \simeq (1 - N)\mu_0 M$ (N is the demagnetization factor, which is approximately constant in the central part of the sample). In addition, the mean value of $P(B)$ for a superconductor (ferromagnet) decreases (increases) proportionally to $B_{app} - B_1$.

*alexander.maisuradze@psi.ch

[1] J. G. Bednorz and K. A. Müller, Z. Phys. B **64**, 189 (1986).

[2] C. W. Chu, P. H. Hor, R. L. Meng, L. Gao, Z. J. Huang, and Y. Q. Wang, Phys. Rev. Lett. **58**, 405 (1987).

[3] D. R. Harshman, G. Aeppli, E. J. Ansaldo, B. Batlogg, J. H. Brewer, J. F. Carolan, R. J. Cava, M. Celio, A. C. D. Chaklader, W. N. Hardy, S. R. Kreitzman, G. M. Luke, D. R. Noakes, and M. Senba, Phys. Rev. B **36**, 2386 (1987).

[4] J. H. Brewer *et al.*, Phys. Rev. Lett. **60**, 1073 (1988).

[5] Y. J. Uemura *et al.*, Phys. Rev. B **38**, 909 (1988).

[6] Y. J. Uemura *et al.*, Phys. Rev. Lett. **62**, 2317 (1989).

[7] B. Pümpin, H. Keller, W. Kündig, W. Odermatt, I. M. Savić, J. W. Schneider, H. Simmler, P. Zimmermann, E. Kaldis, S. Rusiecki, Y. Maeno, and C. Rossel, Phys. Rev. B **42**, 8019 (1990).

[8] P. Zimmermann, H. Keller, S. L. Lee, I. M. Savić, M. Warden, D. Zech, R. Cubitt, E. M. Forgan, E. Kaldis, J. Karpinski, and C. Krüger, Phys. Rev. B **52**, 541 (1995).

[9] J. L. Tallon, C. Bernhard, U. Binninger, A. Hofer, G. V. M. Williams, E. J. Ansaldo, J. I. Budnick, and Ch. Niedermayer, Phys. Rev. Lett. **74**, 1008 (1995).

[10] T. M. Riseman, J. H. Brewer, K. H. Chow, W. N. Hardy, R. F. Kiefl, S. R. Kreitzman, R. Liang, W. A. MacFarlane, P. Mendels, G. D. Morris, J. Rammer, J. W. Schneider, C. Niedermayer, and S. L. Lee, Phys. Rev. B **52**, 10569 (1995).

[11] P. A. Lee, N. Nagaosa, and X.-G. Wen, Rev. Mod. Phys. **78**, 17 (2006).

[12] J. P. Franck, in *Physical Properties of High Temperature Superconductors IV*, edited by D. M. Ginsberg (World Scientific, Singapore, 1994), p. 189.

[13] G. M. Zhao, K. Conder, H. Keller, and K. A. Müller, J. Phys. Condens. Matter **10**, 9055 (1998).

[14] D. Rubio Temprano, J. Mesot, S. Janssen, A. Furrer, K. Conder, H. Mutka, and K. A. Müller, Phys. Rev. Lett. **84**, 1990 (2000).

[15] G. M. Zhao, H. Keller, and K. Conder, J. Phys. Condens. Matter **13**, R569 (2001).

[16] R. Khasanov, A. Shengelaya, K. Conder, E. Morenzoni, I. M. Savić, and H. Keller, J. Phys.: Condens. Matter **15**, L17 (2003); R. Khasanov, A. Shengelaya, K. Conder, E. Morenzoni, I. M. Savić, and H. Keller, J. Phys.: Condens. Matter **16**, S4439 (2004).

[17] H. Keller, in *Superconductivity in Complex Systems*, edited by K. A. Müller and A. Bussmann-Holder, Structure and Bonding Vol. 114 (Springer-Verlag, Berlin, 2005), pp. 114–143.

[18] R. Khasanov, S. Strässle, K. Conder, E. Pomjakushina, A. Bussmann-Holder, and H. Keller, Phys. Rev. B **77**, 104530 (2008).

[19] R. Khasanov, A. Shengelaya, D. Di Castro, E. Morenzoni, A. Maisuradze, I. M. Savić, K. Conder, E. Pomjakushina, A. Bussmann-Holder, and H. Keller, Phys. Rev. Lett. **101**, 077001 (2008).

[20] H. Keller, A. Bussmann-Holder, and K. A. Müller, Mater. Today (Oxford, UK) **11**, 38 (2008).

[21] M. Mali, J. Roos, H. Keller, J. Karpinski, and K. Conder, Phys. Rev. B **65**, 184518 (2002).

[22] A. Eckardt and M. Lewenstein, Phys. Rev. A **82**, 011606(R) (2010).

[23] M. Calamiotou, A. Gantis, E. Siranidi, D. Lampakis, J. Karpinski, and E. Liarokapis, Phys. Rev. B **80**, 214517 (2009).

[24] W. A. Harrison, *Electronic Structure and the Properties of Solids* (Freeman, San Francisco, 1980).

[25] R. Ofer, A. Keren, O. Chmaissem, and A. Amato, Phys. Rev. B **78**, 140508(R) (2008).

[26] J. S. Schilling and S. Klotz, in *Physical Properties of High Temperature Superconductors*, edited by D. M. Ginsberg (World Scientific, Singapore, 1992), Vol. 3.

[27] H. Takahashi and N. Mori, in *Studies of High Temperature Superconductors*, edited by A. V. Narlikar (Nova Science, New York, 1996), Vol. 16.

[28] C. C. Almasan, S. H. Han, B. W. Lee, L. M. Paulius, M. B. Maple, B. W. Veal, J. W. Downey, A. P. Paulikas, Z. Fisk, and J. E. Schirber, Phys. Rev. Lett. **69**, 680 (1992).

[29] S. Rusiecki, B. Bucher, E. Kaldis, E. Jilek, J. Karpinski, C. Rossel, B. Pümpin, H. Keller, W. Kündig, T. Krekels, and G. Van Tendeloo, J. Less-Common Met. **164**, 31 (1990).

[30] I. D. Parker and R. H. Friend, J. Phys. C **21**, L345 (1988).

[31] C. Murayama, Y. Iye, T. Enomoto, N. Mori, Y. Yamada, T. Matsumoto, Y. Kubo, Y. Shimakawa, and T. Manako, Physica C **183**, 277 (1991).

[32] R. P. Gupta and M. Gupta, Phys. Rev. B **51**, 11760 (1995).

[33] J. J. Neumeier and H. A. Zimmermann, Phys. Rev. B **47**, 8385 (1993).

[34] G. G. N. Angilella, R. Pucci, and F. Siringo, Phys. Rev. B **54**, 15471 (1996).

[35] E. V. L. de Mello and C. Acha, Phys. Rev. B **56**, 466 (1997); E. V. L. de Mello, Physica B **265**, 142 (1999).

[36] X. J. Chen, H. Q. Lin, and C. D. Gong, Phys. Rev. Lett. **85**, 2180 (2000).

[37] S. Sarkar, Phys. Rev. B **57**, 11661 (1998).

[38] D. Di Castro, R. Khasanov, A. Shengelaya, K. Conder, D.-J. Jang, M.-S. Park, S.-I. Lee, and H. Keller, J. Phys.: Condens. Matter **21**, 275701 (2009).

[39] R. Khasanov, J. Karpinski, and H. Keller, J. Phys.: Condens. Matter **17**, 2453 (2005).

[40] R. Khasanov, T. Schneider, R. Brütsch, D. Gavillet, J. Karpinski, and H. Keller, Phys. Rev. B **70**, 144515 (2004).

[41] R. Khasanov, T. Schneider, and H. Keller, Phys. Rev. B **72**, 014524 (2005).

[42] S. J. Blundell, Contemp. Phys. **40**, 175 (1999).

[43] J. E. Sonier, J. H. Brewer, and R. F. Kiefl, Rev. Mod. Phys. **72**, 796 (2000); J. E. Sonier, Rep. Prog. Phys. **70**, 1717 (2007).

[44] A. Maisuradze, A. Shengelaya, B. I. Kochelaev, E. Pomjakushina, K. Conder, H. Keller, and K. A. Müller, Phys. Rev. B **79**, 054519 (2009).

[45] I. M. Fita, R. Puzniak, W. Paszkowicz, A. Wisniewski, N. A. Doroshenko, and V. P. Dyakonov, Phys. Rev. B **66**, 014519 (2002).

[46] E. H. Brandt, Phys. Rev. B **37**, 2349 (1988).

[47] E. H. Brandt, Phys. Rev. B **68**, 054506 (2003).

[48] W. Barford and J. M. F. Gunn, Physica C **156**, 515 (1988).

[49] I. V. Fesenko, V. N. Gorbunov, and V. P. Smilga, Physica C **176**, 551 (1991).

[50] Here, $P(B') = \delta(B' - B_{app})$ is the δ function and $\int \delta(B' - B_{app}) \cos(\gamma_\mu B' t + \phi) dB' \equiv \cos(\gamma_\mu B_{app} t + \phi)$. The total asymmetry of the GPS spectrometer was $A_1 + A_2 = 0.204$ with a negligible background component $A_2/A_1 = 0.03$.

[51] R. Khasanov, S. Strässle, D. Di Castro, T. Masui, S. Miyasaka, S. Tajima, A. Bussmann-Holder, and H. Keller, Phys. Rev. Lett. **99**, 237601 (2007).

[52] R. Khasanov, A. Shengelaya, A. Maisuradze, F. La Mattina, A. Bussmann-Holder, H. Keller, and K. A. Müller, Phys. Rev. Lett. **98**, 057007 (2007).

[53] D. Xu, S. K. Yip, and J. A. Sauls, Phys. Rev. B **51**, 16233 (1995).

[54] C. H. Choi and P. Muzikar, Phys. Rev. B **39**, 11296 (1989).

[55] P. J. Hirschfeld and N. Goldenfeld, Phys. Rev. B **48**, 4219 (1993).

[56] H. Kim, G. Preosti, and P. Muzikar, Phys. Rev. B **49**, 3544 (1994).

[57] K. Ohishi, R. H. Heffner, G. D. Morris, E. D. Bauer, M. J. Graf, J.-X. Zhu, L. A. Morales, J. L. Sarrao, M. J. Fluss, D. E. MacLaughlin, L. Shu, W. Higemoto, and T. U. Ito, Phys. Rev. B **76**, 064504 (2007).

[58] M. Tinkham, *Introduction to Superconductivity* (Krieger, Malabar, FL, 1975).

[59] M. I. Larkin, A. Kinkhabwala, Y. J. Uemura, Y. Sushko, and G. Saito, Phys. Rev. B **64**, 144514 (2001).

[60] A. Sahiner, E. D. Crozier, D. T. Jiang, and R. Ingalls, Phys. Rev. B **59**, 3902 (1999).

[61] R. P. Feynman, R. B. Leighton, and M. Sands, *The Feynman Lectures on Physics*, definitive ed. (Pearson Addison Wesley, San Francisco, 2006).

[62] [http://www.srim.org].